Physics of Fluids

RESEARCH ARTICLE | DECEMBER 01 1989

Numerical calculation of stable three-dimensional tertiary states in grooved-channel flow

Cristina H. Amon; Anthony T. Patera

Check for updates

Phys. Fluids 1, 2005–2009 (1989)
https://doi.org/10.1063/1.857473

View Online
Export Citation

01 May 2024 16:14:45

Physics of Fluids

Special Topic: K. R. Sreenivasan:
A Tribute on the occasion of his 75th Birthday

Submit Today

AIP Publishing

AIP Publishing

Numerical calculation of stable three-dimensional tertiary states in grooved-channel flow

Cristina H. Amon[a] and Anthony T. Patera
Department of Mechanical Engineering, Massachusetts Institute of Technology, Cambridge, Massachusetts 02139

(Received 14 April 1988; accepted 21 June 1989)

Numerical simulations of the early transition process in periodic grooved-channel flow are presented. For Reynolds numbers, $R < R_{c,1} = O(100)$, the two-dimensional steady flow is stable to all disturbances; at $R = R_{c,1}$ the flow undergoes a supercritical Hopf bifurcation to a nonlinear two-dimensional steady-periodic state; for $R > R_{c,2} > R_{c,1}$ the wavy two-dimensional flow is unstable to a classical linear three-dimensional secondary instability; and for some range of Reynolds number above $R_{c,2}$ the secondary instability saturates in a steady-periodic, three-dimensional, low-order equilibrium. The three-dimensional equilibria owe their existence and stability to the *narrow band* nature of grooved-channel-flow secondary instability, which in turn reflects the low-Reynolds-number *supercritical* form of the grooved-channel-flow primary bifurcation. The contrast between the low-order, weak transition in "inflectional" complex-geometry channels and the abrupt, snap-through transition in (subcritical-primary broadband-secondary) planar channels illustrates the important role of primary criticality in the early transition process.

I. INTRODUCTION

A large number of free and wall-bounded shear flows undergo transition to turbulence through three-dimensional secondary instability of two-dimensional vortical arrays. Secondary instability has been identified in a wide range of flows, including free shear layers,[1,2] plane Poiseuille flow,[3,4] pipe and plane Couette flows,[3] and boundary layer flow.[3,5] An elegant and complete understanding of the vortex tilting and stretching responsible for secondary instability has recently been achieved by inviscid[6,7] and viscous[8,9] analysis of the stability of elliptical-streamline unbounded flows.

Although secondary instability is a universal feature of wall-bounded shear flow transition, this does not imply that all flows undergoing secondary instability share a common route to turbulence. In this paper we show that it is the relative stability and criticality of the two-dimensional primary bifurcation that is largely responsible for determining whether the transition to turbulence is broadband and abrupt, as in plane Poiseuille flow, or low dimensional and ordered. This conjecture is verified in a controlled fashion by modification of the primary bifurcation character of plane Poiseuille flow through geometric perturbation. Although the results presented are for the particular case of grooved-channel flow,[10,11] the theory is applicable to a large class of inflection-inducing complex-geometry internal flows.[12]

The outline of the paper is as follows. In Sec. II we present the problem formulation and briefly describe our numerical methods. In Sec. III we review the stability of plane Poiseuille flow. Last, in Sec. IV we discuss the linear and nonlinear three-dimensional stability of grooved-channel flow.

[a] Current address: Department of Mechanical Engineering, Carnegie Mellon University, Pittsburgh, Pennsylvania 15213.

II. PROBLEM FORMULATION

We consider incompressible flow in the periodically grooved channel shown in Fig. 1.[10,11] The flow is assumed to be fully developed in the streamwise direction x, and homogeneous in the spanwise coordinate z. We scale all velocities by $\frac{3}{2}V$, where V is the cross-channel average velocity,

$$V = \lim_{W\to\infty} (4hW)^{-1} \int_{-W}^{W} \int_{\partial D_B}^{\partial D_T} u(x,y,z,t)\,dy\,dz,$$

and all lengths by the channel half-width h. Here W is the effectively infinite spanwise extent of the channel. Hereinafter all variables are assumed to be nondimensional. The governing equations are then given by

$$\mathbf{v}_t = \mathbf{v}\times\boldsymbol{\omega} - \nabla\Pi + R^{-1}\nabla^2\mathbf{v}, \quad \text{in } D \tag{1a}$$

$$\nabla\cdot\mathbf{v} = 0, \quad \text{in } D, \tag{1b}$$

where the domain D is defined by the periodicity length between grooves L, the length of the grooves l, and the depth of the grooves a. Here $\mathbf{v}(\mathbf{x},t) = u\hat{\mathbf{x}} + v\hat{\mathbf{y}} + w\hat{\mathbf{z}}$ is the velocity, $\mathbf{x}$ and t represent space and time, respectively, Π is the total pressure, $\boldsymbol{\omega}$ is the vorticity, $\boldsymbol{\omega} = \nabla\times\mathbf{v}$, and $R = \frac{3}{2}Vh/\nu$ is the Reynolds number, where ν is the kinematic viscosity of the fluid. The results presented in this paper are for the particular geometry $L = 5.0$, $l = 3.0$, and $a = 1.68$.

The fully developed boundary conditions for the velocity $\mathbf{v}(\mathbf{x},t)$ are,

$$\mathbf{v}(\mathbf{x},t) = 0, \quad \text{on } \partial D, \tag{2a}$$

$$\mathbf{v}(x + nL,y,z,t) = \mathbf{v}(x,y,z,t), \tag{2b}$$

where n is an integer periodicity index. All calculations reported here are for $n = 1$; the possibility of subharmonic instabilities is discussed in detail in Refs. 10 and 11. For the pressure we require

$$\Pi(\mathbf{x},t) = -f(t)x + \tilde{\Pi}(\mathbf{x},t), \tag{3a}$$

$$\tilde{\Pi}(x + nL,y,z,t) = \tilde{\Pi}(x,y,z,t), \tag{3b}$$

01 May 2024 16:14:45

 0899-8213/89/122005-05$01.90 © 1989 American Institute of Physics

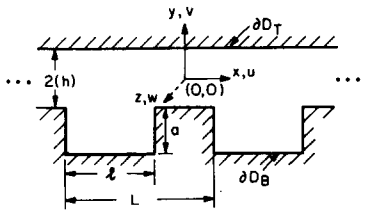

FIG. 1. Geometry of the periodic grooved channel. The domain boundary ∂D comprises the lower grooved wall ∂D_B and the top flat wall ∂D_T.

where the driving pressure gradient $f(t)$ is determined by the imposed flow rate condition

$$Q = \lim_{W\to\infty} (2W)^{-1} \int_{-W}^{W} \int_{\partial D_B}^{\partial D_T} u(x,y,z,t)\,dy\,dz = \frac{4}{3}. \qquad (4)$$

All variables are assumed periodic in the homogeneous spanwise direction.

In order to solve (1) we use periodicity and symmetry in z to write the velocity and pressure as Fourier expansions,

$$\begin{bmatrix} u(\mathbf{x},t) \\ v(\mathbf{x},t) \\ w(\mathbf{x},t) \\ \Pi(\mathbf{x},t) \end{bmatrix} = \begin{bmatrix} u^{(2)}(x,y,t) \\ v^{(2)}(x,y,t) \\ w^{(2)}(x,y,t) \\ \Pi^{(2)}(x,y,t) \end{bmatrix} + \sum_{m=1}^{M} \begin{bmatrix} u_m^{(3)}(x,y,t)\cos m\beta z \\ v_m^{(3)}(x,y,t)\cos m\beta z \\ w_m^{(3)}(x,y,t)\sin m\beta z \\ \Pi_m^{(3)}(x,y,t)\cos m\beta z \end{bmatrix}, \qquad (5)$$

where β is the wavenumber in the spanwise direction. For the analysis of two-dimensional flow the $\mathbf{v}_m^{(3)}$ are identically zero; for the analysis of linear three-dimensional stability we include a single, infinitesimally small, spanwise mode; and for the case of nonlinear three-dimensional flow M is taken sufficiently large so as to include all excited spanwise scales of motion. For the analysis of two-dimensional linear stability $\mathbf{v}^{(2)}$ is further decomposed into a time-independent solution and an infinitesimal perturbation.

The expansions (5) are inserted into the Navier–Stokes equations (1), and the resulting set of Galerkin equations for the $\mathbf{v}^{(2)}(x,y,t)$, $\mathbf{v}_m^{(3)}(x,y,t)$ are discretized in time using an explicit third-order Adams–Bashforth scheme for the convective terms and an implicit Euler-backward splitting method for the Stokes problem.[13] The spatial operators in (x,y) are then discretized by a variational spectral element method,[14–16] yielding a linear algebraic set of equations, which is solved at each time step by static-condensation direct solvers.[17] Various tests are performed to verify the fidelity of the resulting numerical code, several examples of which are given in Refs. 10–12. We note that initial-value-problem time-evolution solvers are used in all aspects of our work: in finding steady or steady-periodic states; in calculating the linear stability of these steady or unsteady equilibria; and in following the nonlinear evolution and saturation of unstable perturbations.

III. REVIEW OF PLANE POISEUILLE FLOW

In order to more clearly understand the grooved-channel results we begin with a brief review of early transition in ($a = 0$) plane Poiseuille flow.[3,4] First, as regards linear stability, the parabolic laminar velocity profile is inviscidly stable because of a lack of inflection.[18] The parabolic profile is, however, viscously unstable to Tollmien–Schlichting traveling waves for Reynolds numbers greater than $R_{c,1}^{P} = 5772$[19]; these instability waves are two dimensional at criticality because of Squire's theorem.[20] Second, investigation of the nonlinear two-dimensional Navier–Stokes equations demonstrates the existence of finite-amplitude Tollmien–Schlichting-like traveling waves of (root-mean-square) amplitude $A_{2\text{-D}}^{P,\text{eq}}$. This primary bifurcation is strongly subcritical (threshold amplitude $A_{2\text{-D}}^{P,2\text{-D thr}}$), with nonlinear two-dimensional equilibria possible for $R > R_{c,2}^{P} = 2900$,[21] and viscous-time scale "quasiequilibria" persisting to even lower Reynolds numbers.[3] Third, it is found that these finite-amplitude two-dimensional waves are linearly unstable to three-dimensional disturbances. This secondary instability is due to the stretching of three dimensionally "tilted" mean vorticity by the finite-eccentricity elliptic vortex flow associated with the two-dimensional nonlinear traveling waves.[3,6–9]

Three-dimensional secondary instability explains many of the features of experimentally observed natural transitions: the critical Reynolds number for secondary instability is $R_{c,3}^{P} \cong 1000$, in good agreement with the experimental transition Reynolds number (this comparison is, perforce, less than conclusive because of the decay of the two-dimensional quasiequilibria); the secondary instability is inviscid in nature, giving convective-time scale growth rates; the instability is intrinsically three dimensional. Perhaps most importantly, the characteristics of secondary instability suggest a plausible explanation for the abrupt nature of plane Poiseuille flow transition, as we now describe.

We begin by artificially constructing a family of two-dimensional wavy flows comprising the parabolic profile and a wavy two-dimensional disturbance (say, of Tollmien–Schlichting form) of root-mean-square amplitude $A_{2\text{-D}}^{P}$.[3] It is then possible to calculate the three-dimensional secondary instability Floquet growth rate as a function of spanwise wavenumber and two-dimensional amplitude, $\sigma_{3\text{-D}}^{P}(\beta, A_{2\text{-D}}^{P})$, and to determine the two-dimensional threshold amplitude $A_{2\text{-D}}^{P,3\text{-D thr}}$ for which $\sigma_{3\text{-D}}^{P} > 0$ for some β. This calculation reveals that $A_{2\text{-D}}^{P,3\text{-D thr}}$ is significantly less than the two-dimensional self-sustaining equilibrium amplitude, $A_{2\text{-D}}^{P,\text{eq}}$. Thus, when the three-dimensional instability is subject to a two-dimensional equilibrium flow of amplitude $A_{2\text{-D}}^{P,\text{eq}}$, large-growth-rate and broadband spanwise excitation will occur. The broadband nature (large spanwise-wavenumber viscous cutoff) of the instability is further accentuated by the high Reynolds numbers associated with the primary bifurcation. These phenomena are illustrated by the $\sigma_{3\text{-D}}^{P}(\beta, A_{2\text{-D}}^{P,\text{eq}})$ curve at $R = 4000$, shown in Fig. 2 of Ref. 3.

It is the relative stability of the two- and three-dimensional components of secondary instability that is responsible for the abrupt transition in plane Poiseuille flow, in that it

01 May 2024 16:14:45

precludes a route to turbulence in which the three-dimensional excitation enters gradually in Reynolds number. In particular, a nonlinear three-dimensional flow will obtain only if either the initial three-dimensional energy is sufficiently large to sustain a deficient two-dimensional flow, or if the two-dimensional flow is sufficiently energetic to be self-sustaining for some appreciable time (i.e., at least as large as $A_{2\text{-D}}^{P,2\text{-D thr}}$). The former, by definition, involves significant three-dimensional nonlinear interactions, whereas the latter will result in explosive, broadband three-dimensional excitation by the arguments of the preceding paragraph; neither initial condition is conducive to a weak, low-dimensional transition process.

IV. GROOVED-CHANNEL FLOW

We now show how the addition of grooves (or other inflection-inducing geometric perturbations) to a planar channel significantly changes the near-critical transition process. We begin with a review of the two-dimensional theory.[10–12] The linear critical Reynolds number for the onset of unsteadiness in our particular grooved-channel geometry is $R_{c,1} \cong 320$, which is dramatically lower than the corresponding value for plane Poiseuille flow. We demonstrate the source of this low critical Reynolds number by plotting in Fig. 2 the steady flow $\partial u^{(2)}/\partial y$ profile at the center groove at $R = 250$, in which it is seen that the groove shear layer creates a strong local inflection point (vorticity extremum). Despite the low critical Reynolds number and strong inflection point, the stability modes are very Tollmien–Schlichting-like in form (compare Figs. 4 and 14 of Ref. 10). Indeed, the dispersion relation for the least stable grooved-channel mode is very close to the plane channel Orr–Sommerfeld dispersion relation.[10–12]

The addition of grooves to a plane channel not only significantly destabilizes the native plane-channel Tollmien–Schlichting waves, but also drastically changes their bifurcation behavior. We plot in Fig. 3 the root-mean-square fluctuation velocity in grooved-channel flow as a function of the Reynolds number, from which it is clear that the flow undergoes a *supercritical* regular Hopf bifurcation at $R = R_{c,1}$. As might be expected from grooved-channel linear theory, the nonlinear two-dimensional grooved-channel flows are very similar to their plane Poiseuille flow counterparts, as can be

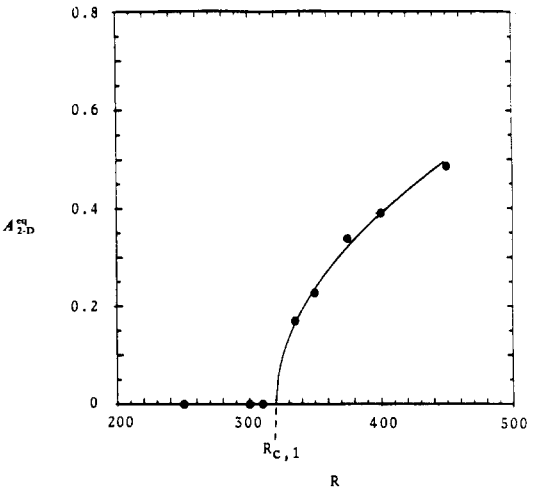

FIG. 3. Root-mean-square amplitude of the fluctuation streamwise velocity at $x = 2.5$, $y = 0.563$ for two-dimensional unsteady grooved-channel flow. The best-fit power law to the amplitude curve, $A = C \cdot (R - R_{c,1})^{\gamma}$, yields an exponent of $\gamma = 0.514$.

seen by comparison of Fig. 24 of Ref. 10 with Fig. 1 of Ref. 3. It is clear that grooved-channel flows are ideally suited to illustrate the effect of primary bifurcation on secondary instability and transition, in that the addition of grooves significantly alters the primary bifurcation behavior of plane Poiseuille flow while simultaneously preserving many of the dynamical features of the parent planar flow. For purposes of understanding the three-dimensional results, we plot in Fig. 4 the streamlines of the two-dimensional unsteady flow at $R = 400$ at one instant in time.

The fact that grooved-channel flows closely resemble plane-channel flows despite very different critical conditions is readily understood by noting that an inflection-inducing small geometric modification may be considered a small dynamic perturbation, *except* as regards growth rate. A small geometric disturbance to plane-channel flow can have a very significant effect on the sign of the growth rate because of the fact that the plane-channel Tollmien–Schlichting wave growth rate is itself viscously small. Thus it is possible to affect the point and form of criticality while altering the global structure of the flow very little. (We believe that the primary instability is viscous in nature despite the low critical Reynolds number, as if this were not the case the Toll-

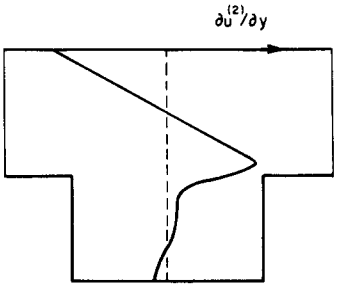

FIG. 2. A plot of $\partial u^{(2)}/\partial y(x = 2.5, y)$ for stable steady two-dimensional grooved-channel flow at $R = 250$. The dashed line indicates the x location of the plot, as well as the zero reference for $\partial u/\partial y$.

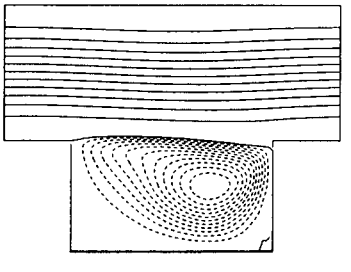

FIG. 4. Streamlines of the steady-periodic two-dimensional secondary flow at $R = 400$ at one instant in time.

01 May 2024 16:14:45

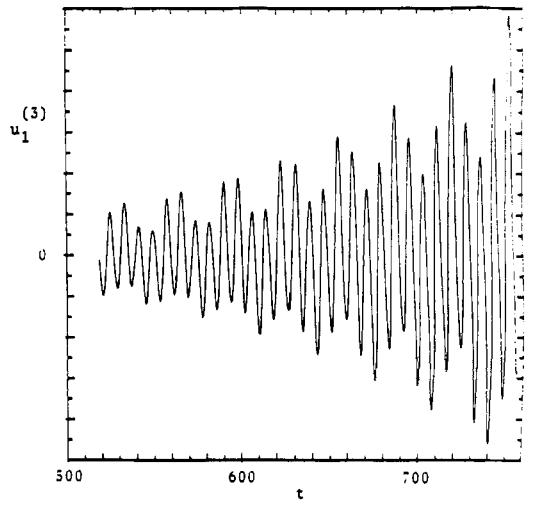

FIG. 5. Three-dimensional infinitesimal perturbation velocity, $u_1^{(3)}$ $(x = 0.5, y = 0.125, t)$, as a function of time at $R = 400$, $\beta = 2.0$.

mien–Schlichting-wave characteristcs would not appear in grooved-channel flow.)

From the similarity of the secondary flows in planar and grooved channels we expect that secondary instability will occur in grooved-channel flow.[22] We show this to be the case by plotting in Fig. 5, $u_1^{(3)}$ $(x = 0.5, y = 0.125, t)$ for $\beta = 2.0$, obtained from direct numerical simulation of the three-dimensional Navier–Stokes equations linearized about the steady-periodic two-dimensional flow at $R = 400$. The critical Reynolds number for three-dimensional growth is $R_{c,2} = 340 > R_{c,1}$; for $R < R_{c,2}$ all linear three-dimensional perturbations decay. The two-dimensional nature of the primary bifurcation is not surprising, given that the steady flow is nearly parallel.

In Fig. 6 we plot the spatial distribution of the three-dimensional instability of Fig. 5 at several times during the flow period T of the two-dimensional secondary flow. The plots of the two-dimensional flow in Fig. 4 and the three-dimensional instability in Fig. 6 at $t = 4T/6$ represent the same physical time. It can be seen that the three-dimensional excitation occurs in the neighborhood of the two-dimensional vortex, that is, at the crest of the two-dimensional streamlines. The location and traveling wave nature of the three-dimensional excitation indicate that the source of this three-dimensional instability is the channel traveling wave, not the groove vortex or shear layer, thus implicating classical (but slightly "detuned") channel secondary instability as the probable cause of growth. In plane Poiseuille flow the three-dimensional excitation takes the form of a staggered array in (x,y); this is not seen in the grooved-channel flow because the wavy two-dimensional flow is slightly stronger on the groove side of the channel.[23]

Although the ubiquity of the secondary instability in complex geometry flow is certainly interesting, of greater interest is the nature of the resulting three-dimensional nonlinear flow. In Fig. 7 we plot the Floquet growth rate $\sigma_{3\text{-D}}(\beta)$ (obtained approximately from initial-value solutions such as Fig. 5) for various Reynolds numbers. As the

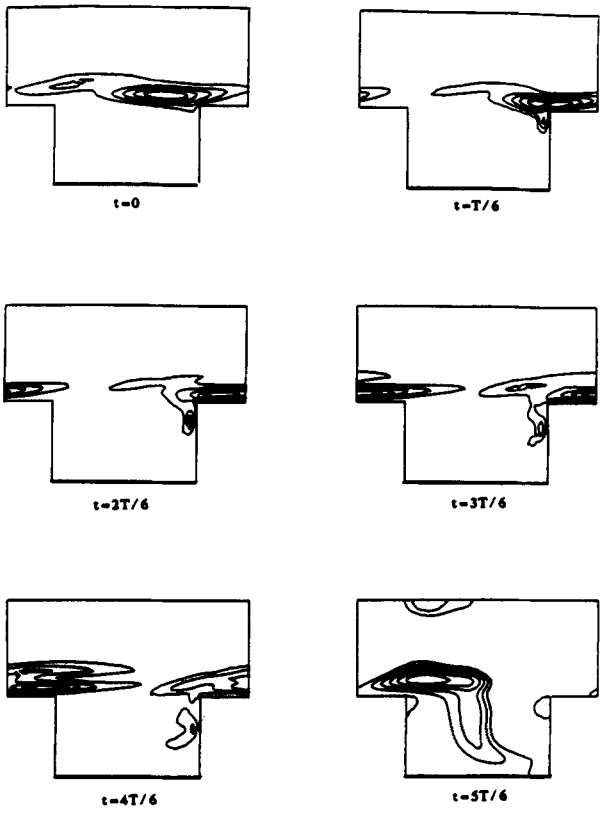

FIG. 6. Contours of $[(u_1^{(3)})^2 + (v_1^{(3)})^2 + (w_1^{(3)})^2]^{1/2}$ (x,y,t) of the three-dimensional linear instability at $R = 400, \beta = 2.0$ at several times during the two-dimensional flow period T.

two-dimensional bifurcation is supercritical, $A_{2\text{-D}}^{eq}$ increases gradually from zero, and as a result the three-dimensional growth-rate curve rises above $\sigma = 0$ in a continuous and narrow band fashion. The relatively low $R_{c,2}$ insures that even in the case of positive growth the high-wavenumber viscous cutoff limits small-scale excitation. These results suggest that at sufficiently low $R - R_{c,2}$ a nonlinear three-dimensional low-order equilibrium should exist, in marked contrast to plane Poiseuille flow.

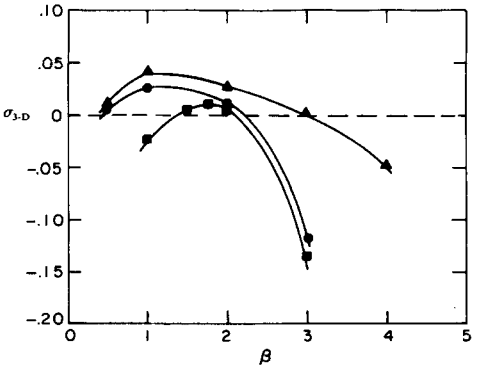

FIG. 7. Growth rate (real Floquet exponent) $\sigma_{3\text{-D}}$ of the linear three-dimensional grooved-channel perturbation at $R = 350$ (■), $R = 400$ (●), and $R = 450$ (▲), as a function of spanwise wavenumber β.

01 May 2024 16:14:45

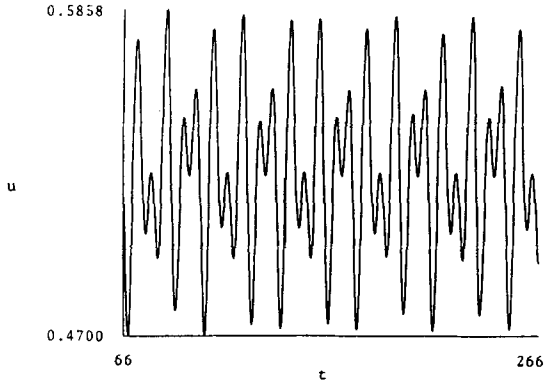

FIG. 8. Streamwise velocity for the fully nonlinear three-dimensional grooved-channel flow, $u(x=2.5,y=0.563,z=0,t)$, as a function of time for $R=350,\beta=2$ $(M=3)$.

This is, indeed, the case. We plot in Fig. 8 the velocity $u(x=2.5,y=0.563,z=0,t)$ for $R=350,\beta=2$ $(M=3)$ resulting from the long-time solution of the full nonlinear three-dimensional Navier–Stokes equations. In Fig. 9 we show the phase portrait of v vs u at the same point in space. The solution is stable and physically realizable (within the assumption of $\beta=2$ periodicity in z and $n=1$ periodicity in x), as it is the result of an evolution, not equilibrium, calculation. At this very low $(R-R_{c,2})$ and judiciously chosen β, the flow appears periodic in time; the folds in the phase portrait and slight changes in the time signal are undoubtedly due to slowly disappearing transients. The flow is also spacially low order, $\|\mathbf{v}_2^{(3)}\| \ll \|\mathbf{v}_1^{(3)}\|$, as would be expected from the narrow band nature of the originating instability.

It should be noted that in plane-channel flow the primary/secondary instability decomposition reveals the physics of transition, however, the natural transition process does not actually follow the ordered sequence of the analysis because of the subcritical character of the flow. In contrast, we conjecture that many complex-geometry flows will faithfully follow the primary/secondary sequence because of the

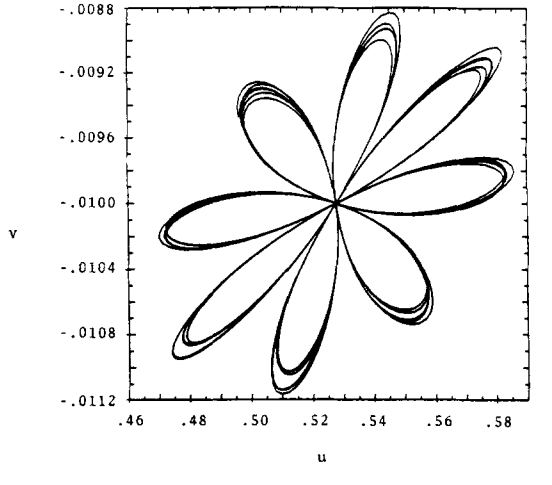

FIG. 9. Phase portrait of v vs u for the nonlinear three-dimensional grooved-channel flow at $R=350,\beta=2$ $(M=3)$ at the point $x=2.5,y=0.563,z=0$.

supercritical form of the primary bifurcation. A corollary to this statement is the ironic result that the classical entities of plane Poiseuille flow (Tollmien–Schlichting waves, fundamental and subharmonic secondary instabilities) may be more readily isolated and observed in complex geometries than in plane channels.

V. CONCLUSIONS

The abrupt transition in plane Poiseuille flow is due to a large growth rate, broadband-secondary instability engendered by a subcritical primary bifurcation. The same cast of plane Poiseuille flow characters, namely, finite-amplitude Tollmien–Schlichting waves and three-dimensional secondary instability, also play a central role in grooved-channel flow transition. In grooved-channel flows, however, the geometry-induced shear layer destabilization yields a low-Reynolds-number supercritical primary instability, resulting in a very different (e.g., Taylor–Couette-like[24]) narrow band transition near criticality.

ACKNOWLEDGMENTS

We would like to acknowledge many helpful discussions with Dr. George Em Karniadakis. The calculations were performed on the NASA Project NAS CRAY-2 computer.

This work was supported by a Venezuelan CONICIT Fellowship (C.H.A.), by the NSF under Grant No. CBT 85-06146, and by the ONR and DARPA under Contract No. N00014-85-K-0208.

01 May 2024 16:14:45

[1] R. T. Pierrehumbert and S. E. Widnall, J. Fluid Mech. **114**, 59 (1982).
[2] R. W. Metcalfe, S. A. Orszag, M. E. Brachet, S. Menon, and J. Riley, J. Fluid Mech. **184**, 207 (1987).
[3] S. A. Orszag and A. T. Patera, J. Fluid Mech. **128**, 347 (1983).
[4] T. Herbert, Phys. Fluids **26**, 871 (1983).
[5] T. Herbert, AIAA Paper No. 84-0009, 1984.
[6] R. T. Pierrehumbert, Phys. Rev. Lett. **57**, 2157 (1986).
[7] B. J. Bayly, Phys. Rev. Lett. **57**, 2160 (1986).
[8] A. D. D. Craik and W. O. Criminale, Proc. R. Soc. London Ser. A **406**, 13 (1986).
[9] M. J. Landman and P. G. Saffman, Phys. Fluids **30**, 2339 (1987).
[10] N. K. Ghaddar, K. Z. Korczak, B. B. Mikic, and A. T. Patera, J. Fluid Mech. **163**, 99 (1986).
[11] N. K. Ghaddar, M. Magen, B. B. Mikic, and A. T. Patera, J. Fluid Mech. **168**, 541 (1986).
[12] G. E. Karniadakis, B. B. Mikic, and A. T. Patera, J. Fluid Mech. **192**, 365 (1988).
[13] S. A. Orszag and L. C. Kells, J. Fluid Mech. **96**, 159 (1980).
[14] A. T. Patera, J. Comput. Phys. **54**, 468 (1984).
[15] K. Z. Korczak and A. T. Patera, J. Comput. Phys. **62**, 361 (1986).
[16] Y. Maday and A. T. Patera, in *State of the Art Surveys on Computational Mechanics*, edited by A. K. Noor and J. T. Oden (ASME, New York, 1989), p. 71.
[17] A. T. Patera, J. Comput. Phys. **65**, 474 (1986).
[18] Lord Rayleigh, Proc. London Math. Soc. **11**, 57 (1880).
[19] S. A. Orszag, J. Fluid Mech. **50**, 689 (1971).
[20] H. B. Squire, Proc. R. Soc. London Ser. A **142**, 621 (1933).
[21] T. Herbert, in *Proceedings of the 5th International Conference of Numerical Methods in Fluid Dynamics*, edited by A. I. van de Vooren and P. J. Zandbergen (Springer, New York, 1976), p. 235.
[22] G. E. Karniadakis and C. H. Amon, in *Proceedings of the 6th IMACS International Symposium on Partial Differential Equations* (1987), p. 525.
[23] C. H. Amon, Sc.D. thesis, Massachusetts Institute of Technology, 1988.
[24] G. P. King, Y. Li, W. Lee, H. L. Swinney, and P. S. Marcus, J. Fluid Mech. **141**, 365 (1984).